

J. Mol. Biol.

Novel Inhibitor for Prolyl Tripeptidyl Aminopeptidase from *Porphyromonas gingivalis* and Details of Substrate-Recognition Mechanism*

Running Title: Prolyl Tripeptidyl Aminopeptidase from *P. gingivalis*

Yue Xu[§], Yoshitaka Nakajima[§], Kiyoshi Ito[¶], Heng Zheng, Hiroshi Oyama[†], Ulrich Heiser[‡], Torsten Hoffmann[‡], Ulf-Torsten Gärtner[‡], Hans-Ulrich Demuth[‡], and Tadashi Yoshimoto

Graduate School of Biomedical Sciences, Nagasaki University, 1-14 Bunkyo-machi, Nagasaki 852-8521, Japan, [‡]Probiodrug AG, Weinbergweg 22 / Biocenter D-06120 Halle (Saale) Germany

[¶]Corresponding Author: Kiyoshi Ito, E-mail: k-ito@nagasaki-u.ac.jp,

Tel: +81-95-819-2435, Fax: +81-95-819-2478

Summary

A new inhibitor, H-Ala-Ile-pyrrolidin-2-yl boronic acid, was developed as an inhibitor against prolyl tripeptidyl aminopeptidase with the K_i value of 88.1 nM. The structure of the prolyl tripeptidyl aminopeptidase complexed with the inhibitor (enzyme-inhibitor complex) was determined at 2.2 Å resolution. The inhibitor was bound to the active site through a covalent bond between Ser603 and the boron atom of the inhibitor. This structure should closely mimic the structure of the reaction-intermediate between the enzyme and substrate.

We previously proposed that two glutamate residues, Glu205 and Glu636, are involved in the recognition of substrates. In order to clarify the function of these glutamate residues in substrate recognition, three mutant enzymes, E205A, E205Q, and E636A were generated by site-directed mutagenesis. The E205A mutant was expressed as an inclusion body. The E205Q mutant was expressed in soluble form, but no activity was detected for it.

Here, the structures of the E636A mutant and its complex with the inhibitor were determined. The inhibitor was located at almost the same position as in the wild-type enzyme-inhibitor complex. The amino group of the inhibitor interacted with Glu205 and the main-chain carbonyl group of Gln203. In addition, a water molecule in the place of Glu636 of the wild-type enzyme interacted with the amino group of the inhibitor. This water molecule was located near the position of Glu636 in the wild type and formed a hydrogen bond with Gln203. The k_{cat}/K_M values of the E636A mutant toward the two substrates used were smaller than those of the wild type by two

orders of magnitude. The K_i value of our inhibitor for the E636A mutant was 48.8 μM , which was 554-fold higher than that against the wild-type enzyme. Consequently, it was concluded that Glu205 and Glu636 are significant residues for the N-terminal recognition of a substrate.

Keywords: prolyl tripeptidyl aminopeptidase, peptidase family S9, serine enzyme, substrate-recognition mechanism, crystal structure

INTRODUCTION

The Gram-negative anaerobe *Porphyromonas gingivalis* is a major pathogen associated with adult periodontitis. *P. gingivalis* possesses a complex proteolytic system, which is very important for its growth and evasion of host defense mechanisms¹⁻³.

Prolyl tripeptidyl aminopeptidase (PTP) from *P. gingivalis* was first identified by Banbula and colleagues⁴. PTP belongs to the family S9, also known as the prolyl oligopeptidase (POP) family, which includes, among other members, POP, dipeptidyl aminopeptidase IV (DPIV), acylaminoacyl peptidase, and oligopeptidase B. POP family enzymes have an Asp-His-Ser catalytic triad occurring in the order of Ser-Asp-His in the primary sequence, with the catalytic serine located within the Gly-X-Ser-X-Gly motif. These features are indications of an α/β -hydrolase topology⁵.

PTP releases a tripeptide Xaa-Xaa-Pro from substrates possessing an N-terminal free amino group and proline residue at the third position from the N-terminus. The enzyme is a homodimer of subunits whose molecular weight is approximately 82,300 and is a type II membrane-bound enzyme. In order to clarify the substrate-recognition mechanism of PTP, we have investigated the enzyme using kinetics and X-ray crystallography.

Recently, we determined the crystal structures of PTP with an N-terminal truncation of 38 residues (PTP39) and its S603A mutant enzyme complexed with the substrate, Gly-Ala-Pro- β -naphthylamide ($-\beta$ NA), at 2.1 and 2.9 Å resolution,

respectively⁶. The subunit of the enzyme is composed of two domains, the N-terminal eight-bladed β -propeller domain (Glu45–Lys470) and the C-terminal catalytic domain (Asn471–Leu732). The active site is located in a large cavity between the two domains. The overall structure of PTP39 was similar to those of mammalian DPIV (PDB code: 1JQP, 1N1M, 1ORV and 1ORW) that release a dipeptide from an oligopeptide with a proline as the second residue from the N-terminus. In DPIV, the N-terminal amino group of a substrate is recognized by two glutamate residues from the N-terminal β -propeller domain, Glu205 and Glu206. In PTP39, however, only Glu205 corresponding to Glu206 in DPIV was conserved. It was considered that Glu636, which belongs to the catalytic domain, is specifically involved in the recognition of the N-terminal amino group of substrates.

A specific inhibitor would be not only a useful tool for the analysis of catalytic mechanism but could also serve as a starting template for potential drug development. Several inhibitors have been synthesized for proline-specific peptidases, and the structures of their enzyme-inhibitor complexes have been analyzed: prolyl aminopeptidase with 5-Prolyl-2-*tert*-butyl-[1, 3, 4]-oxadiazole (Pro-TBODA), Ala-TBODA, and Sarcosinyl-TBODA^{7, 8}; POP with Z-Pro-prolinal⁹; DPIV with diprotin A¹⁰, 1-(2*S*-cyanopyrrolidin-1-yl)-3-(3-iodophenyl)-1-oxopropan-2-aminium trifluoroacetate¹¹, 2-amino-3-methyl-1-pyrrolidine-1-yl-butan-1-one¹², 7-Benzyl-1, 3-dimethyl-8-piperazin-1-yl-3, 7-dihydro-purine-2, 6-dione, *tert*-butyl-Gly-L-Pro-L-Ile, 4-(2-aminoethyl)-benzene sulfonyl fluoride, and L-Pro-boro-L-Pro¹³; and aminopeptidase P with Apstatin¹⁴ and Pro-Leu¹⁵. However, no specific inhibitors of

PTP have been developed.

In this study, we developed a new inhibitor of PTP, H-Ala-Ile-pyrrolidine-2-yl boronic acid, and determined the crystal structure of its complex with the PTP39. Additionally, based on the crystal structure and the kinetic analysis of the E636A mutant, the substrate-recognition mechanism, especially the function of the Glu636 residue, was elucidated.

RESULTS

Kinetic study of the PTP39 and E636A mutant

Kinetic parameters were estimated using Gly-Ala-Pro- β NA and Ala-Phe-Pro- β NA as substrates (Table 1). The K_M values of PTP39 toward Gly-Ala-Pro- β NA and Ala-Phe-Pro- β NA were 0.42 and 0.17 mM, respectively, and those of the E636A mutant were 0.38 and 0.85 mM, respectively. The K_M values of the E636A mutant were similar to those of PTP39. However, since the k_{cat} values of the E636A mutant were significantly lower, the k_{cat}/K_M values were 0.83% and 0.27% of those of PTP39 toward Gly-Ala-Pro- β NA and Ala-Phe-Pro- β NA, respectively.

Inhibition activity of H-Ala-Ile-pyrrolidin-2-yl boronic acid

The K_i values of H-Ala-Ile-pyrrolidin-2-yl boronic acid for PTP39 and the E636A mutant were estimated using Ala-Phe-Pro- β NA as a substrate, and were 88.1 nM and 48.8 μ M, respectively. We also assayed the inhibition activity against prolyl oligopeptidase from *Aeromonas hydrophila*, dipeptidyl aminopeptidase IV from

Stenotrophomonas maltophilia and prolyl aminopeptidase from *Bacillus coagulans* using Ala-Phe-Pro- β NA, Gly-Pro- β NA, and Pro- β NA as substrates, respectively. The H-Ala-Ile-pyrrolidin-2-yl boronic acid did not influence the enzyme activity of either dipeptidyl aminopeptidase IV or prolyl aminopeptidase at concentrations up to 10 μ M. In contrast, prolyl oligopeptidase was significantly inhibited by this concentration, and the estimated K_i value was found to be 127 nM using .Z-Gly-Pro- β NA as a substrate.

Quality of the structure

The refined model of PTP39 complexed with the inhibitor (PTP39-inhibitor complex) consisted of 659 residues, 332 water molecules, a sulfate anion, and an inhibitor molecule with an R -factor of 18.6% at 2.20 \AA resolution. This model lacks the 33 N-terminal residues (12 artificial residues including His-tag and Leu39–Phe49) and 24 other residues (Ala77–Gln83, Glu98–Ala107, Pro472–Tyr476, and Ser532–Ser533) due to the lack of an unequivocal Fourier map. Alanine models were applied in the case of Tyr50, Lys76, Lys470, Asn471, and Arg531, since the electron densities corresponding to the side chains of these residues on the Fourier map were weak or not observed at all. The average thermal factor of the main-chain atoms, water molecules, sulfate anion, and inhibitor were 41.2, 39.7, 60.6, and 31.3 \AA^2 , respectively. PROCHECK¹⁶ analysis of stereochemistry revealed that all residues except for Ser603 fell within the generously allowed region of the Ramachandran plot, with 482 residues in the most favored region, 70 residues in the additionally allowed

region, and 3 residues in the generously allowed region.

The model of the E636A mutant consisted of 692 residues, 532 water molecules, a sulfate anion and a glycerol, and the model of E636A mutant complexed with the inhibitor (E636A-inhibitor complex) consisted of 639 residues, 585 water molecules, and the inhibitor. After refinement for the E636A mutant and the E636A-inhibitor complex, *R*-factors of 18.8 and 18.5% were given at 2.00 and 1.95 Å resolution, respectively. Due to the obscure Fourier map, these models of the E636A mutant and E636A-inhibitor complex lacked 52 residues (the 12 N-terminal artificial residues, Leu39–Tyr53, Ala77–Gln83, Glu98–Ala107, Asn471–Asp473, and Arg531–Val534) and 51 residues (the 12 N-terminal artificial residues, Leu39–Tyr53, Ala77–Gln83, Lys101–Thr105, Asn471–Tyr476, and Arg531–Val534), respectively. The average thermal factors of the main-chain atoms and water molecules at the E636A mutant were 35.2 and 40.6 Å², respectively, and those of the main-chain atoms, water molecules and inhibitor at the E636A-inhibitor complex were 33.1, 40.3, and 29.9 Å², respectively.

Overall structures

The overall structures of the PTP39-inhibitor complex, E636A mutant, and E636A-inhibitor complex showed no significant difference with that of PTP39 (Figure 1). The C α positions of the three structures could be superimposed onto that of PTP39⁶ with root-mean-square deviations of 0.16, 0.16, and 0.16 Å, and maximum distances of 1.92, 1.18, and 1.50 Å, respectively. Briefly, every subunit in the

homodimer consists of two domains, the eight-bladed β -propeller domain (Pro51–Lys470) and the catalytic domain (Asn471–Leu732). The active site is composed of residues from both domains and is located at the large cavity in the side-face of the β -propeller domain. Therefore, the active site was exposed to solvent.

Active site in PTP39-inhibitor complex

The ribbon-and-stick diagram of the active site in the PTP39-inhibitor complex is shown in Figure 2a. The inhibitor was bound to the active site with a covalent bond between the hydroxyl oxygen of Ser603 and the boron atom of the inhibitor. Although the inhibitor was used in its racemic form, only the corresponding *R*-configured form was found bound to the active site after considering the $C\alpha$ -position of the pyrrolidine ring. One of the hydroxyl groups of borate formed a hydrogen bond with the hydroxyl group of Tyr518 at a distance of 2.65 Å. We previously reported the structure of the S603A mutant complexed with the substrate Gly-Ala-Pro- β NA (S603A-substrate complex; PDB code: 2dcm)⁶. From the comparison between these two structures, the position of the inhibitor was found closer to the protein than that of the substrate (Figure 3a). In particular, the pyrrolidine ring of the inhibitor corresponding to the proline residue at the P1 position was just buried in the hydrophobic pocket composed of Tyr604, Val629, Trp632, Tyr635, Tyr639, Val680, and Val681. From the comparison with the structure of PTP39, the conformation of Tyr635 and Val680 was changed by the inhibitor binding, resulting in respective shifts of 0.44 and 0.36 Å to enlarge the hydrophobic pocket. The hydroxyl group of Tyr635 made a hydrogen

bond with the carbonyl oxygen of the inhibitor at the P3 position at a distance of 2.63 Å.

A large space was obvious as the S2 site, composed of Glu205, Phe206, Glu 336, Leu338, Pro521, His522, Tyr639, Tyr643, and Arg642. Two salt-bridges between the two domains were formed by Glu205-Arg642 and Glu336-His522. The isoleucyl group of the inhibitor, corresponding to the P2 position, was located in the S2 site, and the C γ atom was located at distances of 3.61 and 3.70 Å from His522 and Tyr639, respectively.

The N-terminal amino group of the inhibitor interacted with the side-chain carboxyl groups of Glu205 and Glu636 and the main-chain carbonyl group of Gln203 at distances of 2.61, 2.74, and 2.77 Å, respectively. Furthermore, as shown in Figure 4a, Glu205 formed a salt-bridge with Arg642 belonging to the catalytic domain, and Glu636 formed hydrogen bonds with the main-chain NH group of Tyr639 and the side-chain amino group of Gln203 belonging to the β -propeller domain.

PTP39 possesses a large groove extended from the active site to the β -propeller domain. The groove is predominantly composed of residues from the β -propeller domain: Glu193-Arg204, Gln228, Lys247-Pro252, His259, and Pro679-Val680. The N-terminal side-chain of the inhibitor faces to this groove. Accordingly, it is considered that the vestibule area of the groove composed of Gln203, Arg204, and Val680 is the S3 site to accommodate an N-terminal side-chain.

Active site in E636A mutant and E636A-inhibitor complex

The positions of the residues in the active site of the E636A mutant and the E636A-inhibitor complex did not differ very much from those of PTP39 and the PTP39-inhibitor complex (Figure 3b). In spite of the alanine substitution for Glu636, the position of the inhibitor in the E636A mutant virtually overlapped to that in the PTP39-inhibitor complex. In the E636A-inhibitor complex, the N-terminal amino group of the inhibitor interacted with the side-chain of Glu205 and the main-chain carbonyl group of Gln203 at distances of 2.67 and 2.67 Å, respectively (Figure 4b). A water molecule was found at the position approximately corresponding to that of the carboxyl group of Glu636. The N-terminal amino group of the inhibitor formed a hydrogen bond with this water molecule, and this water molecule formed another hydrogen bond with the side-chain amino group of Gln203.

DISCUSSION

The inhibitor binding to the active site

We previously determined the structures of PTP39 and its S603A mutant complexed with a substrate, Gly-Ala-Pro-βNA⁶. In that study, we suggested that the Pro residue of substrates is accommodated by a hydrophobic pocket composed of Tyr604, Val629, Trp632, Tyr635, Tyr639, Val680, and Val681, and that the N-terminal amino group is recognized by Glu205 and Glu636. Superimpositions of the structures of the PTP39-inhibitor and S603A-substrate complexes onto that of PTP39 were performed with the least-square method. The inhibitor was bound to the active site with the same manner in the substrate in the S603A-substrate complex. The

N-terminal amino group of the inhibitor was located at a similar position to that of the substrate: the distance between the two relevant atoms was 0.40 Å. The N-terminal amino group was located at distances of 2.62, 2.73, and 2.77 Å from Glu205, Glu636, and the main-chain carbonyl oxygen of Gln203, respectively. While, the pyrrolidine ring of the inhibitor shifted from that of the substrate to a position fixed in the hydrophobic pocket by approximately 1.4 Å on an average. It is considered that the structure of this complex containing the inhibitor strictly bound to the enzyme with a covalent bond resembles the structure of the covalent reaction intermediate between the enzyme and substrates during catalysis. Although the conformation and positions of Tyr604, Val629, Trp632, Tyr639, and Val680 in the PTP39-inhibitor complex were not different from those in PTP39, the hydrophobic pocket was slightly enlarged by the displacement of Tyr635 and Val680. These conformational changes of Tyr635 and Val680 were also found in the E636A-inhibitor complex. Therefore, this induced fit would inherently occur upon the substrate binding.

The location of the S2 site of PTP fit well with that of DPIV, which belongs to the same family (Figure 5a and 5b). PTP shows no specificity for residues at the P2 position; for instance, it has been reported that PTP can hydrolyze substrates containing nonpolar aliphatic (Ala, Gly, Pro, and Val), aromatic (Phe), polar uncharged (Asn), and charged residues (Glu, Arg, and His) at the P2 position^{4,6}. The large space of the S2 site would not limit the kind of residue at the P2 position of substrates.

Function of the glutamate residues at the active site

DPIV releases an N-terminal Xaa-Pro from substrates containing a Pro at the second position from the N-terminus. The N-terminal free amino group of the substrate is recognized by two glutamate residues, Glu205* and Glu206* (the * denotes the residue from DPIV) at the β -propeller domain^{9-12, 17-18}. Glu205* and Glu206* are found in the helix appended to the fourth blade. This region in PTP forms a loop structure, and is three residues shorter than that of DPIV. Only the Glu205 corresponding to Glu206* is conserved within this loop⁶. This Glu205 forms a hydrogen bond with the N-terminal amino group of the inhibitor and forms a salt bridge with Arg642 from the catalytic domain. Two mutant plasmids expressing E205A and E205Q were constructed. However, it was extremely difficult to obtain the E205A enzyme protein in a soluble form. Regarding the E205Q mutant, although a part of the expressed enzyme was able to be purified as a soluble form, no activity was detected using Ala-Phe-Pro- β NA as a substrate (data not shown). These results suggested that the Glu205 may play an important role in proper protein folding and might contribute to stabilization of the PTP structure through the salt bridge with Arg642.

A residue equivalent to Glu205* could not be found in the active site of PTP. In PTP, the Glu636 from the catalytic domain intruded into the active site and formed a salt bridge with the inhibitor. In DPIV, Asp663*, corresponding to Glu636 in PTP, is located just behind Glu206* and seems to push Glu206* forward. It has been reported that dipeptidyl aminopeptidase activity increases in the A647D mutant of human

fibroblast activation protein α (FAP α) and decreases in the D663A mutant of human DPIV, proteins that belong to the same family¹⁹. FAP α is expressed in epithelial cancers and exhibits a dipeptidyl-aminopeptidase activity with 100-fold lower catalytic efficiency compared to DPIV^{20, 21}. Herein, Ala647 is the residue corresponding to the Asp663* residue in DPIV. Accordingly, Asp663* must be an important residue for the catalytic activity of DPIV.

In the E636A-inhibitor complex, the inhibitor is bound to the active site in the same manner in the PTP39-inhibitor complex except for the contribution of Glu636 (Figure 3b and 4b). In the former, instead of Glu636, a water molecule was found near the corresponding position, located at distances of 2.85 and 2.81 Å from the side-chain Gln203 and the inhibitor amino group, respectively. Although the inhibitor was found at the same position in the active site, the K_i value of our newly synthesized inhibitor against the E636A mutant was 554-fold higher than that against PTP39. Since the positions and conformation of residues in the active site largely overlapped between the PTP39-inhibitor and E636A-inhibitor complexes, it was simply considered that the increase in K_i value resulted from the mutation of E636A. Actually, the E636A mutant exhibited very low activity: k_{cat}/K_M values in the E636A mutant were 0.83 and 0.27% those of PTP39 against Gly-Ala-Pro- β NA and Ala-Phe-Pro- β NA, respectively (Table 1). Therefore, Glu636 must be involved in substrate recognition by the interaction with the N-terminal amino group of the substrate.

Design of specific inhibitor against PTP

PTP is considered a potential drug target in treating periodontal disease caused by *P. gingivalis*. The newly synthesized inhibitor of tripeptide boronic acid, H-Ala-Ile-pyrrolidin-2-yl boronic acid, mimics the structure of the substrate of PTP. Peptide boronic acid is known as an inhibitor of serine proteases, and our inhibitor was designed to specifically inhibit the post-proline cleavage. Prolyl amino peptidase (PAP), DPIV, and POP are serine peptidases cleaving the post-proline peptide bond. Our inhibitor exhibits no inhibition activity against either DPIV from *S. maltophilia* and PAP from *B. coagulans*. However, POP from *A. hydrophila* was strongly inhibited by the inhibitor with a K_i value of 127 nM. POP is a proline-specific endopeptidase found in vertebrates, plants, and bacteria, and is similarly composed of two domains: a seven-bladed β -propeller domain and a catalytic domain^{9, 22}. It has been revealed that the side chain of a substrate at the P3 position is accommodated in a space between blade-3 and blade-4 inside the POP (PDB codes: 1e8m and 1e8n)²³. The side chain of the substrate at the P3 position in POP faces the β -propeller domain, and this conformation differs from that of the inhibitor in the PTP39-inhibitor complex (Figure 5). The blade-3 and -4 in POP correspond to the blade-4 and -5 in the PTP, respectively. In PTP, this space is occupied by the loop that contains Glu205 and intrudes from blade-4. The methyl group of the inhibitor at the P3 position faces the large groove formed between blade-3 and blade-4 and is exposed to solvent. Therefore, in the active site of the PTP, there is enough room to accommodate a very bulky side-chain of a substrate at the P3 position. Hence, a more specific inhibitor against PTP may be developed when a bulky functional group is introduced to the

present inhibitor as an N-terminal side-chain instead of Ala.

Materials and Method

Materials

Fast Garnet GBC was obtained from Sigma Chemical Co. DEAE-Toyopearl and Toyopearl HW65C were purchased from Tosoh Co., Tokyo, Japan. *N*-Cyclohexyl-2-aminoethanesulfonic acid (CHES), lithium sulfate monohydrate, and potassium sodium tartrate tetrahydrate, all of which were used for crystallization, were purchased from Nacalai Tesque Inc., Kyoto, Japan. Ala-Phe-Pro-- β NA was purchased from Wako Pure Chemical Industries, Ltd, Osaka, Japan. Other peptides were synthesized according to previously described methods. The pQE30-PTP39 plasmid, which contains the gene of PTP with an N-terminal truncation of 38 residues⁶, and pKF18k plasmid (Takara, Japan) were used for site-directed mutagenesis. *E. coli* M15 (pRep4) (Qiagen) was used for expression. *E. coli* MV1184 (*ara* Δ (*lac-proAB*) *rpsL thi* (ϕ 80 *lacZ* Δ M15) Δ (*srl-recA*)306::Tn10(*tet*^r) F'⁺[*traD36 proAB*⁺ *lacI*^q *lacZ* Δ M15]) was used for screening the mutated plasmid. A Mutan-Super Express Km Kit was purchased from Takara, Japan. The bacteria were grown in Luria-Bertani broth (LB-broth) and N-broth. PTP39⁶, POP from *Aeromonas hydrophila*²⁴, DPIV from *Stenotrophomonas maltophilia*²⁵ and PAP from *Bacillus coagulans*²⁶ were purified as described previously.

Inhibitor (H-Ala-Ile-pyrrolidin-2-yl boronic acid) synthesis.

The tripeptide-boronic acid type inhibitor was synthesized by the method described below (Figure 6). H-Ala-Ile-pyrrolidin-2-yl boronic acid, **5**, was synthesized starting from *N*-Boc-pyrrole, **1**²⁷. Thereby the treatment of **1** with lithium (2, 2, 6, 6)-tetramethylpiperidine (LiTMP) and triethyl borate led to the *N*-Boc-2-pyrrolyl boronic acid, **2**. Subsequent hydrogenation utilizing a Pt/C catalyst and addition of (1*S*, 2*S*, 3*R*, 5*S*)-pinanediol resulted in the protected boronic acid derivative, (1*S*, 2*S*, 3*R*, 5*S*)-pinanediol (Boc-pyrrolidin-2-yl) boronic ester, **3**, as a mixture of diastereomers. After deprotection of the N-terminal Boc-moiety and coupling to the *N*-Boc-protected dipeptide Boc-Ala-Ile-OH, the resulting product, (1*S*, 2*S*, 3*R*, 5*S*)-pinanediol (Boc-Ala-Ile-pyrrolidin-2-yl) boronic ester, **4**, was reacted with phenyl boronic acid. Subsequent deprotection of the N-terminus finally resulted in the inhibitor molecule as a diastereomeric mixture which was not separated. Details of each step follows.

N-Boc-2-pyrrolyl boronic acid, **2**: TMP (4.4 mL, 26 mmol) was dissolved in 140 mL of dry THF and cooled to 198 K. After the addition of *n*BuLi (16.25 mL, 26 mmol), the mixture was stirred for 15 min. A solution of Boc-pyrrole **1** (4.2 mL, 25 mmol) in 10 mL of THF was added dropwise over a period of 10min followed by triethyl borate (15.0 mL, 88 mmol). The solution was stirred for 15 additional min at 198 K and overnight at r.t (room temperature). After that, 200 mL of Et₂O was added and the solution was subjected three treatments with 50 mL of 1M KHSO₄ solution followed by three extractions by means of 50 mL of NaHCO₃ and 50 mL of brine. Then the organic layer was dried and the solvent was evaporated. The remaining oil was used without further purification. Yield: 2.71 g (51%)

(1*S*, 2*S*, 3*R*, 5*S*)-pinanediol (*Boc*-pyrrolidin-2-yl) boronic ester, **3**: Compound **2** (2.65 g, 12.56 mmol) was dissolved in 60 mL of dry ethyl acetate, and 0.3 g of Pt/C (10%) was added. The mixture was placed in an autoclave and hydrogenated utilizing an H₂-pressure of 65bar for 4h. After that, the catalyst was removed by filtration and the solvent was evaporated, 1.44 g (6.7 mmol) of the remaining glass was dissolved in 50 mL of absolute Et₂O, and 1.25 g (7.4 mmol) of (1*S*, 2*S*, 3*R*, 5*S*)-pinanediol was added. The mixture was stirred for 2h at r.t. The remaining oil was used without further purification. Yield: 2.53 g (98%)

(1*S*, 2*S*, 3*R*, 5*S*)-pinanediol (*Boc*-Ala-Ile-pyrrolidin-2-yl) boronic ester, **4**: Compound **3** (4.71 g, 13.5 mmol) was treated with a 160 mL of an ice-cooled saturated solution of HCl in Et₂O. The solution was stirred overnight at r.t. The solvent was evaporated, and the remaining solid was washed by means of 150 mL of a mixture Et₂O/pentane and dried, giving (1*S*, 2*S*, 3*R*, 5*S*)-pinanediol (pyrrolidin-2-yl) boronic ester, hydrochloride salt, the deprotected form of compound **3**, as a white powder. The product was used without further purification. Yield: 3.46 g (90%).

Boc-Ala-Ile-OH (0.30 g, 1 mmol) was dissolved in 9 mL of absolute CHCl₃ and cooled to 5°C. HOBt (0.15 g, 1 mmol) and 1-ethyl-3-(3-dimethylaminopropyl)-carbodiimide hydrochloride (0.19 g, 1.3 mmol) were added, and the mixture was stirred for 30 min. After that, deprotected compound **3** (0.28 g, 1 mmol) and *N*-methyl-morpholine (220 mL, 2 mmol) were added and the mixture was stirred overnight at r.t. 70 mL of CHCl₃ was added and the workup procedure was conducted as usual. The remaining oil was purified by means of

column chromatography, utilizing a CHCl₃/MeOH gradient. Yield: 0.275 g (51%), MS m/z 534.2 [M+H]⁺, 556.3 [M+Na]⁺

H-Ala-Ile-pyrrolidin-2-yl boronic acid, **5**: Compound **4** (0.275g, 0.51mmol) was dissolved in 20mL of an ice-cooled saturated solution of HCl in Et₂O and stirred for 15min at r.t. and additionally 1h at r.t. The white precipitate was filtered off and dried. After that, it was dissolved in 10 mL of 0.1 N aqueous HCl, and phenyl boronic acid (0.076g, 0.60mmol) was added. The mixture was stirred for 2h. Over that period, 7mL of heptane was added, and then removed when stirring was stopped. The organic phases were discarded. The aqueous phase was frozen and lyophilized yielding **5** as a white powder. Yield: 0.052g (30%), MS: m/z 300.2 [M+H]⁺, ESI-FTICR-MS: m/z 326.22473 ([M+H]⁺, calc. for C₁₅H₂₉BN₃O₄⁺ 326.22456, glycol adduct), HPLC (214 nm): r.t. 14.21 min (94.5% HPLC purity), ¹HNMR (500MHz, CD₃OD) δ 0.88-1.02 (m, 7H), 1.15-1.22 (m, 1H), 1.42-1.51 (m, 3H), 1.60-1.68 (m, 2H), 1.83-2.14 (m, 5H), 2.83-3.01 (m, 1/2H), 3.09-3.11 (m, 1/2H), 3.48-3.60 (m, 2H), 3.82-3.86 (m, 1H), 3.94-3.99 (m, 1H), 4.43-4.55 (m, 1H).

Construction of mutant enzyme by site-directed mutagenesis

Site-directed mutation was introduced into the gene by a PCR-based method using the Mutan-Super Express Km Kit (Takara, Japan) following the manufacturer's instructions. Briefly, pQE30-PTP39⁶ was digested by *Bam*HI and *Hind*III, and the 2.1kb fragment containing the gene for PTP39 was subcloned into the same restriction sites of pKF18k to produce pKF18k-PTP39, which was then used as the template to

produce the mutant plasmids, pFK18k-PTP39-E205Q and pKF18k-PTP39-E636A. The oligonucleotides, 5'-TACACCAGCGTCAATTCGGTATC-3' and 5'-AATCGATATGCGATTATGTAC-3', were used as the mutagenic primer for the E205Q and E636A mutants, respectively. The mutations were confirmed by sequencing analysis with a 3100-Avant Genetic Analyzer. DNA fragments containing the specific mutations were prepared by digestion with *KpnI* and *HindIII*, and the resultant fragments were inserted into the same restriction sites of the plasmid pQE30-PTP39 to produce pQE30-PTP39-E205Q and pQE30-PTP39-E636A.

Expression and Purification of E205Q and E636A mutants

E. coli M15 (pRep4) was transformed with the pQE30-PTP39-E636A plasmid. The transformant was grown until A_{600} reached 0.5 at 303 K in 20 liters of N-broth containing 50 $\mu\text{g/ml}$ ampicillin. After the addition of isopropyl- β -thiogalactopyranoside (IPTG) to a concentration of 0.2 mM, the transformant was cultured for an additional 18 h. Approximately 220 mg of the E636A mutant was obtained as a purified protein from the harvested cells (61 g wet weight) using the same methods including column chromatography on Toyoperal HW650C and DEAE-Toyopearl columns (TOSOH) as described for wild-type PTP39⁶. The purity of the isolated enzyme was confirmed by SDS-PAGE. The enzyme solution was dialyzed against 20 mM Tris-HCl buffer (pH7.0) containing 0.2 M potassium chloride, and concentrated to 35 mg/ml using Centriprep YM-30 (Millipore).

The E205Q mutant was prepared in the same manner as that described for E636A except that the plasmid pQE30-PTP39-E205Q was used and the cultivation was carried out at 293 K after the IPTG induction. Approximately 45 mg of the purified E205Q mutant was obtained from the harvested cells (30 g wet weight). The mutant enzyme solution was dialyzed against 0.2 M Potassium chloride with 20 mM Tris-HCl buffer (pH7.0), and concentrated to 32 mg/ml using Centriprep YM-30 (Millipore).

Enzyme activity assay

The activity of the purified enzyme, PTP39-E636A, was assayed using Gly-Ala-Pro- β NA, Ala-Phe-Pro- β NA and Z-Gly-Ala-Pro- β NA as substrates. The reaction mixture (1.0 ml) consisted of 0.8 ml of 20 mM Tris-HCl buffer (pH 7.0), 0.1 ml of enzyme solution, and 0.1 ml of substrate solution. After 10 min incubation at 310 K (unless otherwise indicated), the reaction was stopped by adding 0.5 ml of Fast Garnet GBC (1 mg/ml) solution containing 10% (v/v) Triton X-100 in 1 M sodium acetate buffer (pH 4.0). The absorbance at 550 nm was measured after 20 min. To determine the K_M values, the concentration of substrate was varied. Lineweaver-Burk plots were used to calculate the K_M and apparent V_{max} values. The enzyme concentrations were estimated from the molar extinction coefficient, 11,900. The k_{cat} value was calculated using a molecular mass of 79,393.

Inhibition activity of the synthesized inhibitor

The reaction mixture (1.0 ml) consisted of 0.7 ml of 20 mM Tris–HCl buffer (pH 7.0), 0.1 ml of enzyme solution, and 0.1 ml of inhibitor solution. After incubation at 310 K for 5 minutes, 0.1 ml of the substrate solution was added to initiate the reaction, and incubation for 10 min at 310 K followed. The reaction was terminated by the addition of 0.5 ml Fast Garnet GBC (1 mg/ml) solution containing 10% (v/v) Triton X-100 in 1 M sodium acetate buffer (pH 4.0). The absorbance at 550 nm was measured after 20 min. To determine the K_i value, the concentrations of substrate and inhibitor were varied. Dixon plots were used to calculate K_i values.

Crystallization and data collection

Crystallization of the PTP39 complexed with the inhibitor (PTP39-inhibitor complex) was carried out at 293 K by the hanging-drop vapor-diffusion method. The same volume of the reservoir solution (1.1 M potassium/sodium tartrate, 200 mM lithium sulfate, and 100 mM CHES buffer, pH 9.0) and the protein solution (18 mg/ml enzyme solution containing 2 mM of the inhibitor) were mixed. After 10 days incubation, hexagonal crystals grew to dimensions of 0.2 x 0.2 μ x 0.2 mm; they consisted of isomorphous crystals with a ligand-free enzyme and belonged to the space group $P6_322$ with the following cell dimensions: $a=150.1$, $b=150.1$, $c=161.0$ Å, $\gamma= 120^\circ$. The crystallizations of the E636A mutant complexed with the inhibitor (E636A-inhibitor complex) and the E636A mutant alone were carried out using the same conditions as for PTP39.

The diffraction data for the PTP39-inhibitor complex, the E636A-inhibitor complex

and the E636A mutant were collected to 2.20, 2.00, and 1.95 Å resolution, respectively, at 100 K using a wavelength of 1.000 Å from the synchrotron radiation source. All data were collected by total oscillation range of 180° with the ϕ oscillation of 0.5° using station BL5 at the Photon Factory (Tsukuba, Japan). For data collection under cryogenic conditions, the crystals were soaked for several minutes in a prepared solution containing 30%(v/v) glycerol, 1.1 M potassium sodium tartrate, 200 mM lithium sulfate, and 100 mM CHES buffer (pH 9.0). The crystals were mounted in a nylon loop and flash-cooled at 100 K. All data were processed and scaled by HKL2000²⁸, and are summarized in Table 2.

Structure determination and refinement

The scaling of all data and the map calculations was performed using the CCP4 program suite²⁹, and the model building was performed using the programs XTALVIEW³⁰ and COOT³¹. The coordinate of the ligand-free PTP (PDB code: 2d5l) was used for the initial model-building. The structure of the PTP-inhibitor complex was refined by simulated annealing and energy minimization with the program CNS³² using the data obtained from 20 to 2.20 Å resolution. The structure was examined by inspecting the composite omit map. The difference Fourier map clearly displayed a residual electron density corresponding to the inhibitor bound at the active site. This Fourier map was assigned to *R*-configured form of two diastereomer at the C α -position of the pyrrolidine ring of the inhibitor on the basis of its shape. Refinement using REFMAC²⁹ and model rebuilding were alternately carried out over

several cycles; then water molecules were selected on the basis of the peak height and the distance criteria from the difference map. The water molecules whose thermal factors exceeded 60 Å after refinement were removed from the list. Further model building and refinement cycles gave an *R*-factor of 18.6% and an *R*-free value of 22.0% using 51,107 reflections from 20 to 2.2 Å resolution. The maximal thermal factor of the water molecules was 58.5 Å².

The same refinement procedure was applied to the E636A mutant and the E636-inhibitor complex. The difference Fourier map displayed a residual electron density corresponding to the inhibitor in the E636A-inhibitor complex. In the E636A mutant, the Fourier map showed residual electron density in the hydrophobic pocket, which accommodates a proline residue of the substrate. This residual electron density was assigned to glycerol as a cryoprotectant from size, shape, and peak height. A refinement cycle including simulated annealing and energy minimization, selection of water molecules, and model-rebuilding gave *R*-factors of 18.8 and 18.5 % and *R*-free values of 21.3 and 21.2 % using 66,749 and 72,472 reflections at 20 to 2.0 and 1.95 Å resolutions, with a maximal thermal factors of water molecules of 59.9 and 59.9 Å², respectively.

REFERENCE

1. McBride, B.C., Singh, U., & Joe, A. (1993). *Porphyromonas gingivalis*: Gene cloning of determinants of pathogenicity. In: Genetics and Molecular Biology of Anaerobic Bacteria. pp 552-568. Ed: Madeleine Sebald. Springer-Verlag.

2. Haffajee, A.D., & Socransky, S.S. (1994). Microbial etiological agents of destructive periodontal diseases. *Periodontol.* 2000 **5**, 78-111.
3. Travis, J., Pike, R., Imamura, T., & Potempa, J. (1997). *Porphyromonas gingivalis* as virulence factors in the development of periodontitis. *J. Periodontal. Res.***32**, 120–125.
4. Banbula, A., Mark, P., Bugno, M., Silberring, J., Dubin, A., Nelson D., Travis, J., & Potempa, J. (1999). Prolyl tripeptidyl peptidase from *Porphyromonas gingivalis*. A novel enzyme with possible pathological implications for the development of periodontitis. *J. Biol. Chem.* **274**, 9246-9252.
5. Ollis, D.L., Cheah, E., Cygler, M., Dijkstra, B., Frolow, F., Franken, S.M., Harel, M., Remington, S.J., Silman, I., Schrag, J., Sussman, J. L., Verschueren, K.H.G., & Goldman, A. (1992). The α/β hydrolase fold. *Protein Eng.* **5**, 197–211.
6. Ito, K., Nakajima, Y., Xu, Y., Yamada, N., Onohara, Y., Ito, T., Matsubara, F., Kabashima, T., Nakayama, K., & Yoshimoto, T. (2006). Crystal Structure and Mechanism of Tripeptidyl Activity of Prolyl Tripeptidyl Aminopeptidase from *Porphyromonas gingivalis*. *J. Mol. Biol.* **362**, 228-240.
7. Inoue, T. Ito, K., Tozaka, T., Hatakeyama, S., Tanaka, N., Nakamura, K.T., & Yoshimoto, T. (2003). Novel inhibitor for prolyl aminopeptidase from *Serratia marcescens* and studies on the mechanism of substrate recognition of the enzyme using the inhibitor. *Archives of Biochemistry and Biophysics*, **416**, 147–154.
8. Nakajima, Y., Ito, K., Sakata, M., Xu, Y., Nakashima, K., Matsubara, F., Hatakeyama, S. & Yoshimoto, T. (2006). Unusual Extra Space at the Active Site

- and High Activity for Acetylated Hydroxyproline of Prolyl Aminopeptidase from *Serratia marcescens*. *J. Bacteriol.* **188**, 1599-1606.
9. Fulop, V., Bocskei, Z., & Polgar, L. (1998). Prolyl oligopeptidase: an unusual beta-propeller domain regulates proteolysis. *Cell*, **94**, 161-170.
 10. Thoma, R., Loeffler, B., Stihle, M., Huber, W., Ruf, A., & Henning, M. (2003). Structural Basis of Proline-Specific Exopeptidase Activity as Observed in Human Dipeptidyl Peptidase-IV. *Structure*, **11**, 947-959.
 11. Engel, M., Hoffmann, T., Wagner, L., Wermann, M., Heiser, U., Kiefersauer, R., Huber, R., Bode, W., Demuth H.U., & Brandstetter, H. (2003). The crystal structure of dipeptidyl peptidase IV (CD26) reveals its functional regulation and enzymatic mechanism. *Proc. Natl Acad. Sci. USA*, **100**, 5063–5068.
 12. Rasmussen, H. B., Branner, S., Wiberg, F. C. & Wagtmann, N. (2003). Crystal structure of human dipeptidyl peptidase IV/CD26 in complex with a substrate analog. *Nat. Struct. Biol.* **10**, 19–25.
 13. Engel, M., Hoffmann, T., Manhart, S., Heiser, U., Chambre, S., Huber, R., Demuth, H.U. & Bode, W. (2006). Rigidity and flexibility of dipeptidyl peptidase IV; crystal structures of and docking experiments with DPIV. *J. Mol. Biol.* **355**, 768-783.
 14. Graham, S.C., Maher, M.J., Simmons, W.H., Freeman, H.C. & Guss J.M. (2004). Structure of *Escherichia coli* aminopeptidase P in complex with the inhibitor apstatin. *Acta Crystallogr. D Biol Crystallogr.* **60(10)**, 1770-1779.
 15. Wilce, M. C., Bond, C. S., Dixon, N. E., Freeman, H. C., Guss, J. M., Lilley, P. E.

- & Wilce, J. A. (1998). Structure and mechanism of a proline-specific aminopeptidase from *Escherichia coli*. *Proc. Natl. Acad. Sci. USA*, **95**, 3472-3477.
16. Laskowski, R.A., MacArthur, M.W., Moss, D.S. & Thornton, J.M. (1993). PROCHECK: a program to check the stereochemical quality of protein structures. *J. Appl. Crystallog.* **26**, 283–291.
17. Abbott, C.A., McCaughan, G.W., & Gorrell, M.D. (1999). Two highly conserved glutamic acid residues in the predicted L propeller domain of dipeptidyl peptidase IV are required for its enzyme activity. *FEBS Letters*. **458**, 278-284.
18. Hiramatsu, H., Kyono, K., Higashiyama, Y., Fukushima, C., Shima, H., Sugiyama, S., Inaka, K., Yamamoto, A. & Ahimizu, R. (2003). The structure and function of human dipeptidyl peptidase IV, processing a unique eight-bladed beta-propeller fold. *Biochem. Biophys. Res. Comm.* **302**, 849-854.
19. Aertgeerts, K., Levin, I., Shi, L., Snell, G. P., Jennings, A., Prasad, G. S. *et al.* (2005). Structural and Kinetic Analysis of the Substrate Specificity of Human Fibroblast Activation Protein. *J. Biol. Chem.* **280**, 19441–19444.
20. Garin-Chesa, P., Old, L. J., & Rettig, W. J. (1990). Cell surface glycoprotein of reactive stromal fibroblasts as a potential antibody target in human epithelial cancers. *Proc. Natl. Acad. Sci. USA*, **87**, 7235–7239.
21. Park, J.E., Lenter, M.C., Zimmerman, R.N., Garin-Chesa, P., Old, L.J. & Rettig, W.J. (1999). Fibroblast activation protein, a dual specificity serine protease expressed in reactive human tumor stromal fibroblasts. *J. Biol. Chem.* **274**,

- 36505-36512.
22. Shan, L., Mathews, I.I., & Khosla, C. (2005). Structural and mechanistic analysis of two prolyl endopeptidases: role of interdomain dynamics in catalysis and specificity. *Proc. Natl. Acad. Sci. USA*, **102**, 3599-3604.
 23. Fulop, V., Szeltner, Z., Renner, V., & Polgar, L. (2001). Structure of prolyl oligopeptidase substrate/inhibitor complexes. Use of inhibitor binding for titration of the catalytic histidine residue. *J. Biol. Chem.* **276**, 1262-1266.
 24. Kanatani, A., Yoshimoto, T., Kitazono, A., Kokubo, T., & Tsuru, D. (1993). Prolyl endopeptidase from *Aeromonas hydrophila*: cloning, sequencing and expression of the enzyme gene, and characterization of the expressed enzyme. *J. Biochem. (Tokyo)*. **113**, 790-796.
 25. Kitazono, A., Yoshimoto, T., & Tsuru, D. (1992). Cloning, sequencing, and high expression of the praline iminopeptidase gene from *Bacillus coagulans*. *J. Bacteriol.* **174**, 7919-7925.
 26. Kabashima, T., Ito, K., & Yoshimoto, T. (1996). Dipeptidyl peptidase IV from *Xanthomonas maltophilia*: sequencing and expression of the enzyme gene and characterization of the expressed enzyme. *J. Biochem.* **120**, 1111-1117.
 27. Kelly, T.A., Fuchs, V.U., Perry, C.W., & Snow R.J. (1993) The Efficient Synthesis and Simple Resolution of a Prolineboronate Ester Suitable for Enzyme-Inhibition Studies. *Tetrahedron* **49**, 1009-1016.
 28. Otwinowski. Z. & Minor, W. (1997) Processing of X-ray Diffraction Data Collected in Oscillation Mode. *Methods Enzymol* **276**, 307-329

29. Collaborative Computational Project, Number 4. (1994). The CCP4 suite: programs for protein crystallography. *Acta Crystallog. D Biol. Crystallogr.*, **50**, 760–763.
30. McRee, D.E. (1999). XtalView/Xfit: a versatile program for manipulating atomic coordinates and electron density. *J. Struct. Biol.* **125**, 156–165.
31. Emsley, P., & Cowtan, K. (2004) Coot: model-building tools for molecular graphics. *Acta Crystallog. D Biol. Crystallogr.* **60**, 2126-2132
32. Brunger, A.T., Adams, P.D., Clore, G.M., Delano, W.L., Gros, P., Grosse-Kunstleve, R.W., Jiang, J.-S., Kuszewski, J., Nilges, N., Pannu, N.S., Read, R.J., Rice, L.M., Simonson, T., & Warren, G.L. (1998). Crystallography and NMR System (CNS): A New Software System for Macromolecular Structure Determination. *Acta Crystallog. D Biol. Crystallogr.* **54**, 905-921.
33. Kraulis, P.J. (2004) MOLSCRIPT: A Program to Produce Both Detailed and Schematic Plots of Protein Structures. *J. Appl. Cryst.* **24**, 946-950
34. Merritt, E.A. & Bacon D.J. (1997) Raster3D Photorealistic Molecular Graphics *Methods Enzymol.* **277**, 505-524
35. Fenn, T.D., Ringe, D., & Petsko, G.A. (2003) POVScript+: a program for model and data visualization using persistence of ray-tracing. *J. Appl. Cryst.* **36**, 944-947
36. Wallace, A.C., Laskowski, R.A., & Thornton, J.M. (1995) LIGPLOT: A program to generate schematic diagrams of protein-ligand interactions. *Prot. Eng.*, **8**, 127-134

FIGURE LEGEND

Figure 1 The structure of prolyl tripeptidyl aminopeptidase

(a) One of the dimers of the PTP39-inhibitor complex is shown as a ribbon model and the other is shown as protein-surface model. The α -helices and β -strands from the β -propeller domain are represented by blue and cyan, and those from the catalytic domain are represented by orange and red, respectively. The protein surface is indicated by cyan and orange on the respective domains. This diagram was drawn using the program PYMOL (<http://www.pymol.org/>), MOLSCRIPT³³, and RASTER3D³⁴. (b) Stereo diagram of the β -propeller domain in the PTP39-inhibitor complex from the top view. Each propeller blade is separated by color with numbering. Our synthesized inhibitor is shown as a stick model. (c) A stereo diagram superimposing the subunits of the PTP-inhibitor complex, the E636A mutant, and the E636A-inhibitor complex onto PTP39 (PDB code: 2d5l). The C α traces of PTP39, the PTP39-inhibitor complex, the E636A mutant, and the E636A-inhibitor complex are represented by black, green, blue, and red lines, respectively. The stick models of the inhibitor in the PTP39- and E636A-inhibitor complexes are designated with the same color as each C α -trace lines. Diagram was drawn using the program MOLSCRIPT³³.

Figure 2 The inhibitor bound to the active site with the *F_o-F_c* omit map contoured at 2 σ levels

Ribbon-and-stick models of the active-site structure in the PTP39-inhibitor (a) and E636A-inhibitor (b) complexes. Each inhibitor is shown as a ball-and-stick model. Diagrams were drawn with the program POVSCRIPT⁺ ³⁵ and rendered with the program POVRAY (<http://www.povray.org>).

Figure 3 Stereo diagrams of superimposed structures of the active site in prolyl tripeptidyl aminopeptidase

(a) A ribbon-and-stick model of the active site superimposing the S603A-substrate and PTP39-inhibitor complexes onto PTP39 with the least-square method; the structures are represented by pink, green, and grey, respectively. The substrate and inhibitor are shown as a ball-and-stick model. (b) A ribbon-and-stick model superimposing the E636A mutant and the E636A-inhibitor complex onto the PTP39-inhibitor complex; the structures are represented by blue, red, and green, respectively.

Figure 4 Scheme diagram of the active site binding the inhibitor

These diagrams schematically represent protein-inhibitor interactions in the PTP39-inhibitor (a) and E636A-inhibitor (b) complexes. Diagrams were drawn based on output from the program LIGPLOT³⁶.

Figure 5 Surface diagram of the active site at the POP family

(a) PTP39 complexed with our synthesized inhibitor (b) DPIV complexed with

1-iodo-phenylalanyl-(2*S*)-pyrrolidine-2-yl-methylamine (PDB code: 1orw) (c) S554A mutated POP complex with 6-aminobenzoyl-Gly-Phe-Gly-Pro-Phe-Gly. Surface of the β -propeller and catalytic domains were represented by blue and orange, respectively. These diagrams were drawn using the program PYMOL (<http://www.pymol.org/>).

Figure 6 Scheme of synthesis for H-Ala-Ile-pyrrolidin-2-yl boronic acid

Synthesized inhibitor was mixture of two diastereomers, which differ in the chiral carbon indicated asterisks (*).

FOOT NOTE

The atomic coordinates and structure factors for PTP39 complexd with the inhibitor, E636A mutant, and E636A mutant complexed with the inhibitor (PDB code 2EEP, 2Z3W, 2Z3Z) have been deposited in the Worldwide Protein Data Bank (wwPDB; <http://www.wwpdb.org>), the Protein Data Bank Japan at the Institute for Protein Research in Osaka University (PDBj; <http://www.pdbj.org/>)

**This work was supported in part by the ‘National Project on Protein Structural and Functional Analyses’ run by the Japanese Ministry of Education, Culture, Sports, Science and Technology.*

[§]These authors contributed equally to this work.

[†]Present address: Department of Immunobiology, Nihon Pharmaceutical University,
10281 Komuro, Ina-cho, Kitaadachi-gun, Saitama 362-0806, Japan

¹ The abbreviations used are: PTP, prolyl tripeptidyl aminopeptidase; POP, prolyl oligopeptidase; DPIV, dipeptidyl aminopeptidase IV; PTP39, PTP truncated the 38 N-terminal residues; -- β NA, -- β -naphthykamide; -TBODA, 2-ter-butyl-[1, 3, 4]-oxadiazole; PAP, prolyl aminopeptidase; CHES, *N*-cyclohexyl-2-aminoethansulfonic acid; TMP, (2, 2, 6, 6,)-tetramethylpiperidine; IPTG, isopropyl- β -thiogalactopyranoside;

Table 1 Kinetic parameters of the PTP39 and E636A mutant catalyzed hydrolysis
of fluorogenic substrates

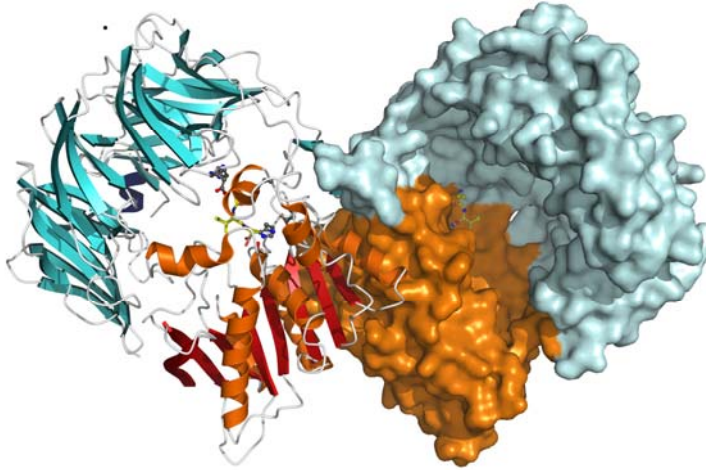
Substrate	PTP39			E636A mutant		
	K_M	k_{cat}	k_{cat}/K_M	K_M	k_{cat}	k_{cat}/K_M
	<i>mM</i>	s^{-1}	$s^{-1}mM^{-1}$	<i>mM</i>	s^{-1}	$s^{-1}mM^{-1}$
Gly-Ala-Pro- β NA	0.42	354	843	0.38	2.65	6.97
Ala-Phe-Pro- β NA	0.17	511	3006	0.85	6.80	8.0

Table 2 Data collection and refinement statistics

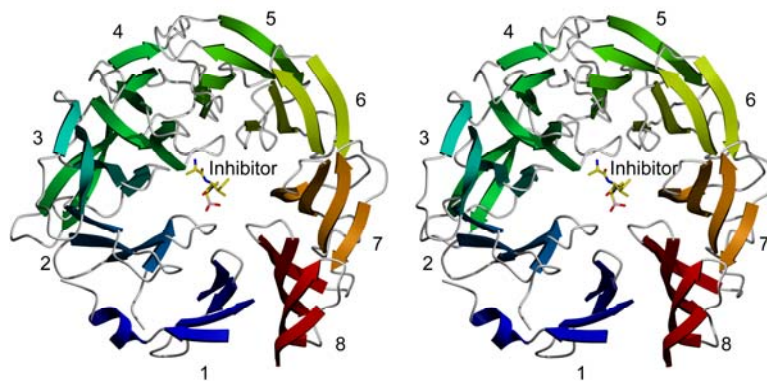
	PTP39-inhibitor complex	E636A mutant	E636A-inhibitor complex
Data collection			
Space group	<i>P</i> 6 ₃ 22	<i>P</i> 6 ₃ 22	<i>P</i> 6 ₃ 22
Cell parameter			
<i>a</i> , <i>b</i> (Å)	150.1	149.7	149.8
<i>c</i> (Å)	161.0	160.9	161.5
Resolution range (Å)	50-2.2 (2.28-2.20)	50-2.0 (2.07-2.00)	50-1.95 (2.02-1.95)
Number of unique reflections	54749 (5385)	71966 (7035)	77828 (7590)
Completeness (%)	99.9 (100)	99.9 (99.6)	99.8 (99.0)
Redundancy	20.8 (19.9)	20.4 (19.5)	20.2 (18.7)
<i>R</i> _{merge}	0.069 (0.281)	0.064 (0.315)	0.062 (0.306)
Mean <i>I</i> /σ(<i>I</i>)	58.3 (9.1)	61.6 (7.5)	64.0 (7.0)
Willson B (Å ²)	37.6	30.9	29.6
Refinement			
Resolution range (Å)	20-2.2	20-2.0	20-1.95
<i>R</i> -factor	0.186	0.188	0.185
<i>R</i> _{free}	0.220	0.213	0.212
Average B-factor			
main chain (Å ²)	41.2	35.2	33.1
side chain (Å ²)	41.8	36.2	34.2
waters (Å ²)	39.7	40.6	40.3
inhibitor (Å ²)	31.3		29.9
<i>R</i> _{merge} = $\sum_{hkl} \sum_i I_{hkl,i} - \langle I_{hkl} \rangle / \sum_{hkl} \sum_i I_{hkl,i}$, where <i>I</i> = observed intensity and $\langle I \rangle$ = average intensity for multiple measurements.			
Values in parentheses refer to the last resolution shell.			

Figure 1

(a)



(b)



(c)

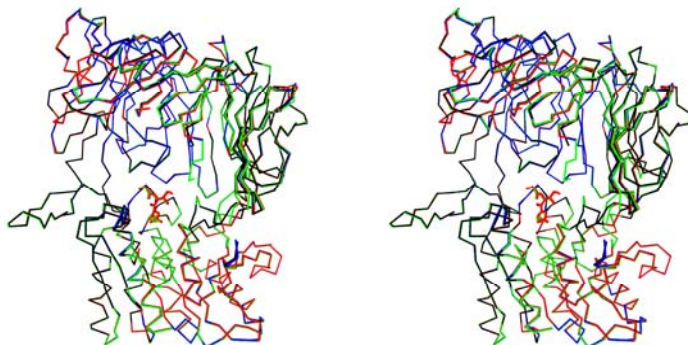


Figure 2

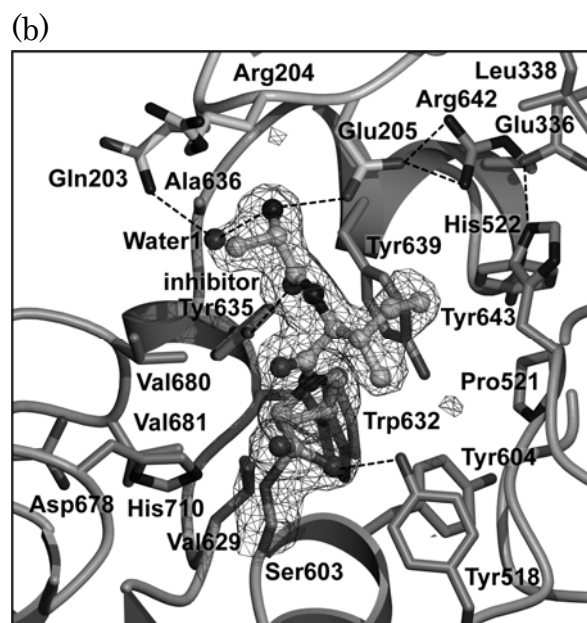
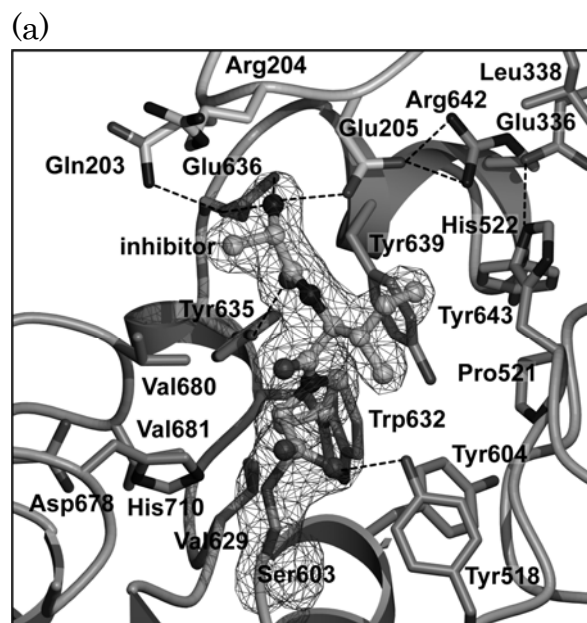
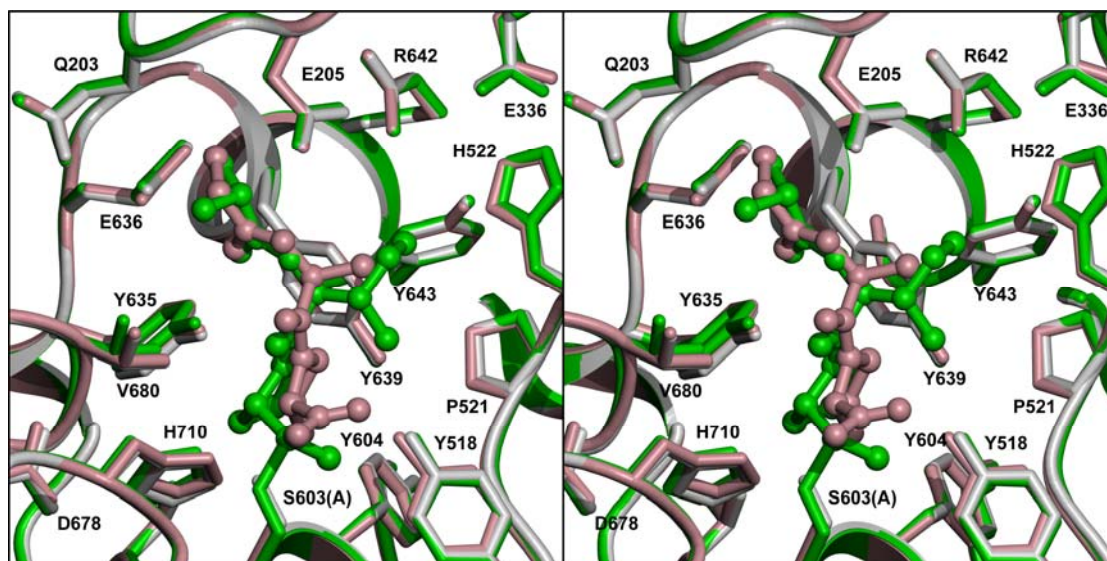


Figure 3

(a)



(b)

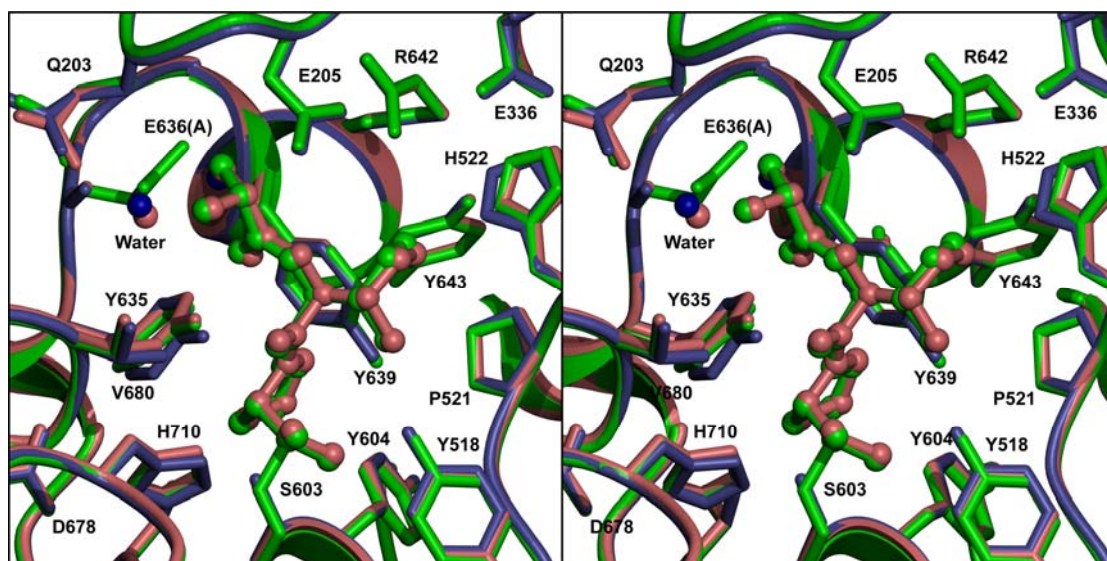
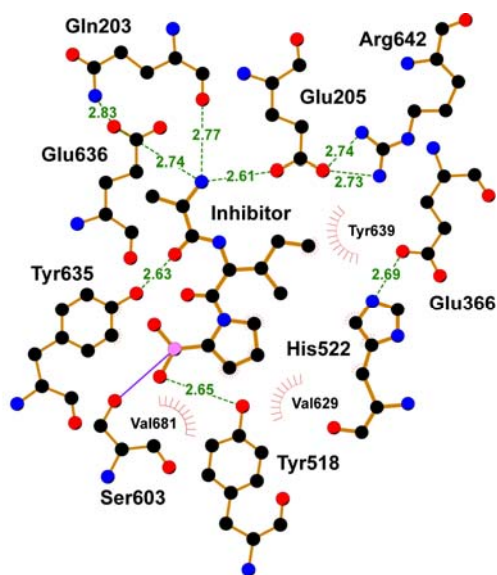


Figure 4

(a)



(b)

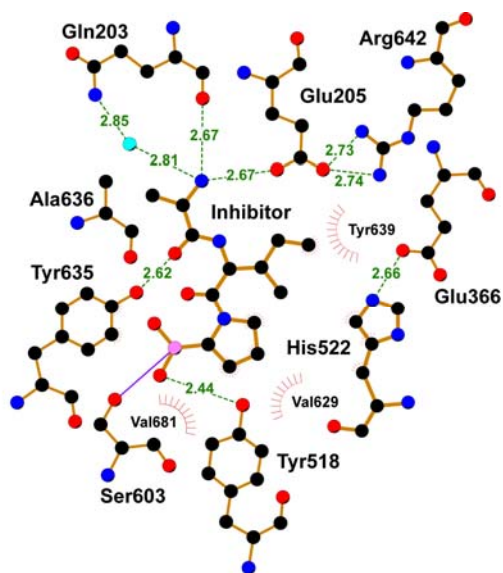


Figure 5

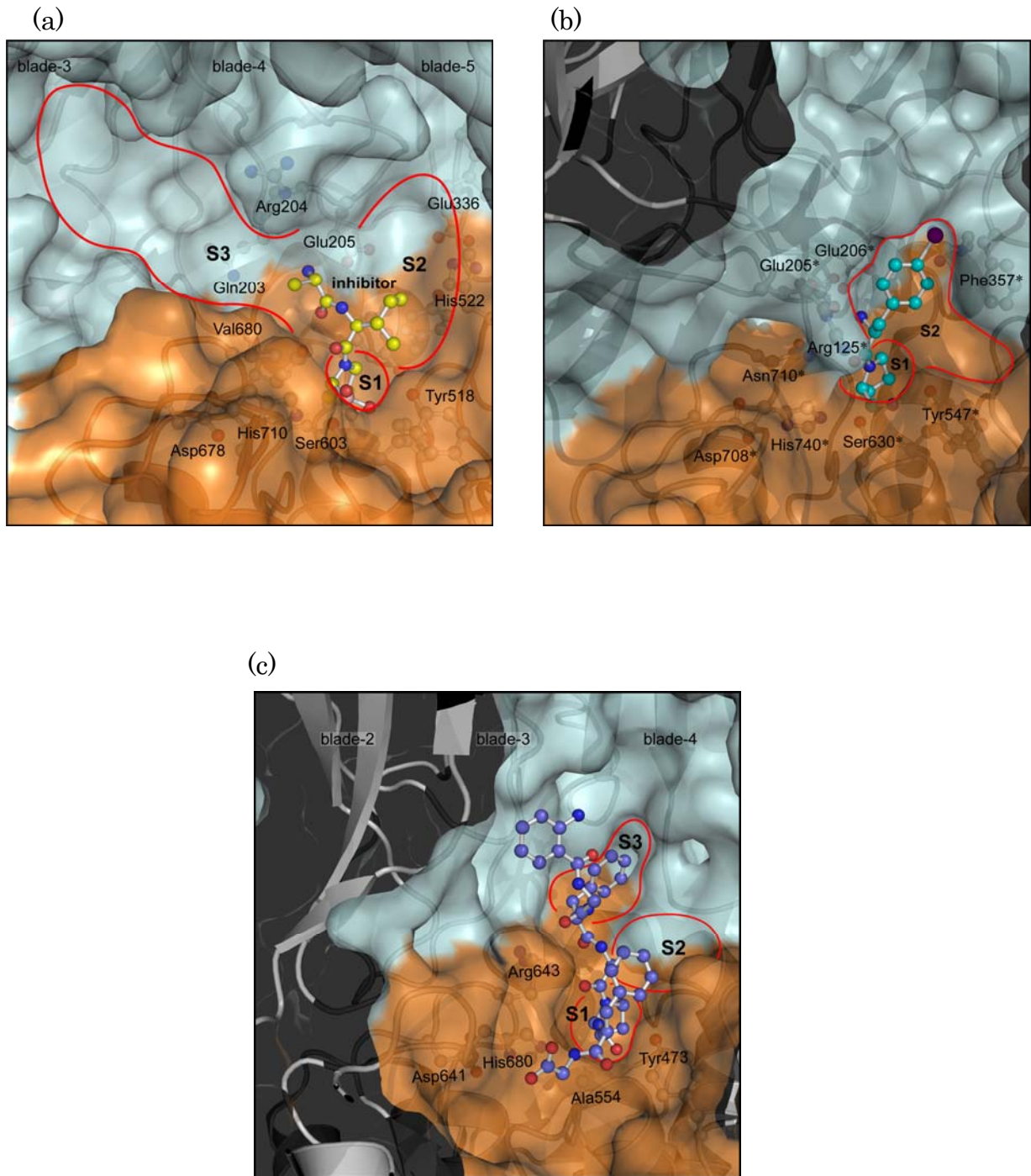


Figure 6

